J Mater Sci: Mater Electron (2025) 36:2147

Theoretical and experimental studies on a semi-organic third-order nonlinear optical material for photonic and optical limiting applications

P. Hemalatha[1], M. Mohanraj[1], M. Lakshmipriya[2], T. C. Sabari Girisun[3], P. Jayaprakash[4], and M. Parthasarathy[1,*]

[1] *Department of Physics, School of Basic Sciences, Vels Institute of Science, Technology and Advanced Studies, Pallavaram, Chennai, Tamil Nadu 600117, India*
[2] *Department of Physics, School of Physical and Chemical Sciences, B. S. Abdur Rahman Crescent Institute of Science and Technology, Vandalur, Chennai, Tamil Nadu, India*
[3] *Nanophotonics Laboratory, School of Physics, Bharathidasan University, Tiruchirappalli, Tamil Nadu 620024, India*
[4] *Department of Physics, St. Joseph's Institute of Technology, OMR, Chennai, Tamil Nadu 600119, India*

Received: 3 October 2025
Accepted: 4 November 2025

ABSTRACT

A good quality third-order nonlinear optical (NLO) single crystal of D-phenylglycine hydrochloride (DPGCL) was successfully synthesised using the solvent evaporation method. Single crystal X-ray diffraction (XRD) analysis confirmed its orthorhombic structure with the space group $P2_12_12_1$. UV–Visible spectroscopy revealed a cut-off wavelength of 228 nm and a band gap of 5.4 eV. For the first time, quantum chemical calculations, including a detailed HOMO–LUMO analysis, were conducted alongside assessments of optical parameters, illustrating excellent crystalline quality. The photoluminescence spectrum exhibited strong ultraviolet light emission. HR-SEM and EDAX analyses provided valuable insights into the crystal's surface morphology and elemental composition. Thermal analysis indicated stability with a melting point of 286 °C, while the laser damage threshold power density was determined to be 5.46 GW/cm^2. The second-harmonic generation (SHG) efficiency of the material was found to be 1.3 times that of potassium dihydrogen phosphate (KDP). Furthermore, the Z-scan technique was employed for the first time to elucidate the third-order NLO properties, yielding an absorption coefficient (β) of 0.87×10^{-10} m/W, a saturation intensity (I_s) of 32×10^{11} W/m^2, and an optical limiting threshold of 2.89×10^{12} W/m^2, thereby demonstrating the crystal's significant potential for nonlinear optical limiting applications. The broad transparency range, combined with exceptional crystalline quality and enhanced laser resistance, underscores the material's potential utility in photonics applications.

Address correspondence to E-mail: mps2k7@gmail.com

https://doi.org/10.1007/s10854-025-16117-8
Published online: 24 November 2025

1 Introduction

In the vibrant field of photonics and optoelectronics, the interaction of nonlinear optical (NLO) processes within different materials is a crucial foundation for developing advanced technologies. The search for innovative NLO materials, carefully designed to meet specific requirements while exhibiting exceptional efficiency, is essential for advancing complex optoelectronic and photonic systems. A notable result of this effort is the emergence of a new class of materials called semi-organics. By combining the high optical nonlinearity and diverse structural features of organic compounds [1] with the excellent thermal stability and strong mechanical properties of inorganic substances [2, 3], these semi-organic materials offer great potential for a wide range of applications. Among this intriguing group, glycine stands out as the simplest amino acid, boasting a broad spectrum of chemical and physical attributes. D-phenylglycine, a noteworthy variant, is classified as a monoamino carboxylic aromatic amino acid characterised by a nonpolar side group. The side groups in this category are inherently hydrophobic [4], imparting distinctive behaviours and functionalities. Notably, it features a benzene ring within its side chain that acts as a vital functional moiety, further enhancing its versatility.

This compound is not only fascinating in its own right but also acts as a vital precursor in the synthesis of β-lactam antibiotics, such as semisynthetic cephalosporins and penicillins [5]. Derivatives of D-phenylglycine, including D-phenylglycinium bromide [6], D-phenylglycinium nitrate [7], D-phenylglycinium perchlorate [8], and Bis(D-phenylglycinium) sulfate monohydrate [9], are currently under intense research due to their interesting physical and chemical properties. Derivatives contain a donor carboxylic acid (COOH) group and a proton acceptor amino (NH_2) group, classifying them as zwitterions. They form strong hydrogen bonds, crucial for non-centrosymmetric structures in effective NLO crystals. These compounds show improved thermal stability, mechanical strength, and excellent optical transmittance.

In the present study, a high-quality single crystal of D-phenylglycine hydrochloride (DPGCL) was successfully synthesised using the slow solvent evaporation technique under optimised conditions. This work is notable for its systematic examination of the relationship between the crystal's molecular structure and its third-order nonlinear optical (NLO) response, which has not been documented in the existing literature, to the best of our knowledge. Comprehensive quantum chemical calculations were conducted, accompanied by a detailed analysis of the highest occupied molecular orbital (HOMO) and the lowest unoccupied molecular orbital (LUMO). These investigations, along with assessments of various optical parameters, underscored the exceptional crystalline quality of the material under consideration. A variety of techniques were employed, including single crystal X-ray diffraction (XRD), ultraviolet–visible (UV–Vis) transmittance studies, determination of various optical constants, photoluminescence (PL) analysis, high-resolution scanning electron microscopy/energy dispersive X-ray analysis (HR-SEM/EDAX), thermogravimetric-differential thermal analysis (TG–DTA), laser damage threshold (LDT) evaluation, and third-order NLO (Z-scan) analysis. The results confirmed the presence of significant optical limiting and nonlinear refractive properties, thereby highlighting the potential applications of DPGCL in photonics and optoelectronic devices. This comprehensive assessment of structural, optical, and NLO properties provides valuable insights for the design of amino acid-based organic crystals intended for electronic and photonic technology applications.

1.1 Experimental procedure

1.1.1 Synthesis and growth

The starting materials for this experiment, D-phenylglycine and hydrochloric acid, were obtained from Sigma-Aldrich with a purity of 99%. To prepare a concentrated solution, D-phenylglycine and hydrochloric acid were mixed in a 1:1 ratio and dissolved in distilled water at 35 °C. The solution was stirred vigorously for six hours to ensure homogeneity. After mixing, the mixture was filtered through Whatman filter paper to remove impurities. The solution was then left undisturbed in a stable environment. After 30 days of gradual evaporation, a good, transparent single crystal of D-phenylglycine hydrochloride measuring $(19 \times 3 \times 2)$ mm^3 was obtained as shown in Fig. 1.

1.1.2 Solubility studies

The solubility of the purified D-phenylglycine hydrochloride was carefully evaluated across various

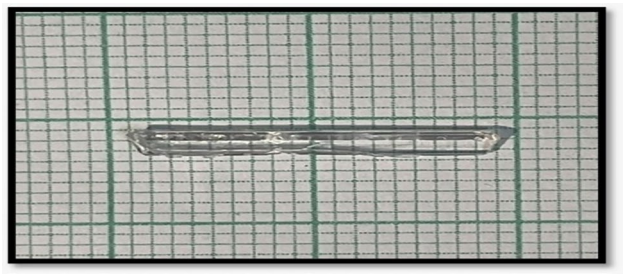

Fig. 1 As-grown single crystal of DPGCL

temperatures using thermogravimetric analysis, as outlined in the previously described methods. The tests were performed at several key temperatures like 35, 40, 45, and 50 °C. The results showed a clear and promising solubility trend, i.e. positive temperature coefficient of solubility, as illustrated in Fig. 2, indicating that the solubility of D-phenylglycine hydrochloride increases significantly with rising temperatures. This trend aligns with the general principles of solute behaviour, as the temperature rises, it usually enhances solvation due to increased molecular movement and kinetic energy within the solution. Additionally, these experiments will further investigate the precise solubility limits at higher temperatures and examine their implications for various industrial applications, potentially opening new avenues for using this compound in chemical processes.

2 Results and discussion

2.1 Single crystal X-ray diffraction analysis

The single-crystal X-ray diffraction analysis of the titled compound was performed using an ENRAF NONIUS CAD4 X-ray diffractometer. Single-crystal XRD analysis was used to determine cell parameters and crystal structure. It confirmed that the crystal belongs to the orthorhombic system with a space group of $P2_12_12_1$. The unit cell parameters are a = 5.452(17) Å, b = 7.278(2) Å, and c = 22.819(1) Å, with $\alpha = \beta = \gamma = 90°$, which align well with the reported data [10] as shown in Table 1.

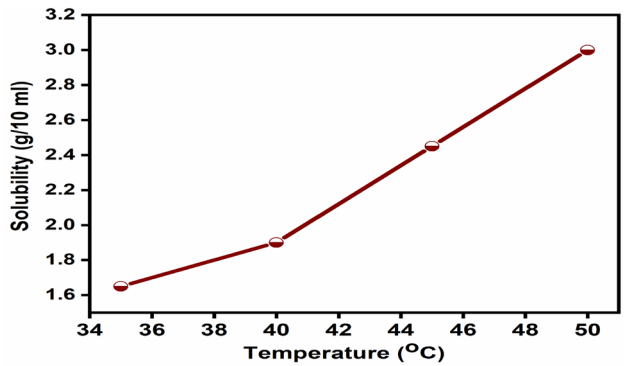

Fig. 2 Solubility curve of DPGCL

2.2 Optical studies

2.2.1 UV–visible transmittance analysis

The UV–visible analysis is used to examine the molecular structure and linear optical properties. However, limited information can be obtained because the absorption of UV and visible light involves promoting electrons from a lower energy state to a higher energy state [11, 12]. The grown material is subjected to transmittance measurements across the wavelength range of 200–800 nm. From the spectrum, it is evident that the material exhibits a low absorbance throughout the visible region, indicating a greater transmittance range. The lower cut-off wavelength is found to be 228 nm, as shown in Fig. 3a, which results from the π-π* transition of the aromatic phenyl ring. To gain deeper insights into its properties, we apply Tauc's relation (1), which serves as an essential framework for calculating the absorption coefficient:

$$(\alpha h\nu)^n = T\left(h\nu - E_g\right) \tag{1}$$

In this equation, the exponent n varies based on the type of bandgap present: $n = 1/2$ indicates a direct bandgap, while $n = 2$ pertains to an indirect bandgap. The resulting Tauc's plot, depicted in the in Fig. 3b, illustrated that the bandgap energy is determined to be 5.4 eV. The wide bandgap energy suggests that the

Table 1 Single-crystal XRD parameters of DPGCL

Lattice parameters	Present work	Ravichandran et al. [10]
a (Å)	5.452(17)	5.437(5)
b (Å)	7.278(2)	7.257(8)
c (Å)	22.819(1)	22.773(2)
$\alpha = \beta = \gamma$ (°)	90	90
Crystal system	Orthorhombic	Orthorhombic
Space group	$P2_12_12_1$	$P2_12_12_1$

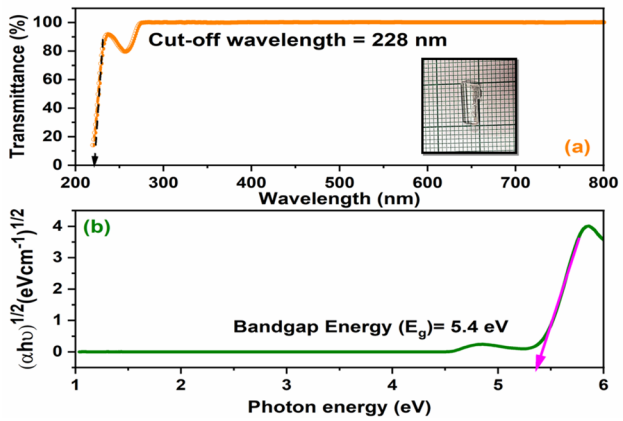

Fig. 3 **a** UV–Visible transmittance, **b** Tauc's plot of DPGCL

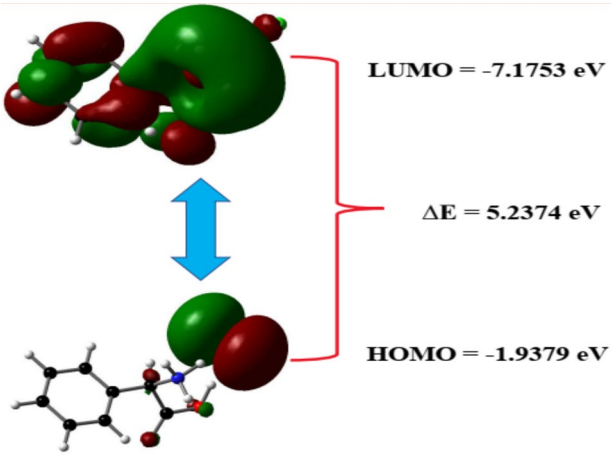

Fig. 4 The atomic orbital compositions of the frontier molecular orbital of the DPGCL

material can withstand laser exposure and is suitable for prominent optical and laser-active applications [13]. These characteristics highlight its potential for developing advanced photonic devices.

2.2.2 *HOMO–LUMO analysis*

The exploration of frontier molecular orbitals (FMOs) is essential in molecular science, as it allows a deeper understanding of the optical and electronic properties of various molecules [14]. These orbitals are crucial for evaluating a molecule's characteristics and behaviour. By analysing excitation energies in a neutral system from a fundamental perspective, one can focus on the potential energy difference between the highest occupied molecular orbital (HOMO) and the lowest unoccupied molecular orbital (LUMO). The HOMO, characterised by its nucleophilic nature, represents the outermost orbital of the molecule. It mainly acts as an electron donor, intrinsically linked to the ionization potential; in other words, it affects the energy needed to remove an electron from the molecule. Conversely, the LUMO exhibits electrophilic properties and functions as the innermost orbital, primarily accepting electrons and being directly related to the molecule's electron affinity. A Density Functional Theory (DFT) calculation was carried out on the specified material using the Gaussian 09 software package. The advanced B3LYP functional was employed in conjunction with the sophisticated 6–311++ G (d, p) basis set to ensure accurate and reliable results [15]. Figure 4 vividly illustrates the energy level plots of the HOMO and LUMO, providing a clear visualisation of their respective energy positions. The energy difference (ΔE) between the HOMO and LUMO is a key indicator of the chemical reactivity and kinetic stability of molecular systems. For example, when examining DPGCL, the HOMO energy is − 7.17 eV while the LUMO energy is − 1.93 eV, resulting in a notable HOMO–LUMO energy gap (ΔE) of 5.23 eV. This energy gap is a crucial factor in predicting the reactivity and stability of the molecular compound. The observations suggest that the optical properties of DPGCL are closely linked to its electronic structure, particularly in terms of charge distribution and transfer between the donor and acceptor regions of the molecule. This significant finding emphasises the substantial potential of the material for nonlinear optical applications [16].

2.2.3 *Molecular electrostatic potential (MEP) analysis*

The molecular electrostatic potential (MEP) serves as a robust descriptor of a molecule's chemical reactivity, structural interactions, and hydrogen bonding behaviour in relation to its environment [17]. Specifically, to identify the reactive sites that may engage in electrophilic and nucleophilic attacks within D-phenylglycine hydrochloride, we present a detailed illustration featuring an iso-electron density surface, enhanced by vivid 3D plots of the MEP surface, as shown in Fig. 5. In this representation, different colour gradients correspond to specific electrostatic potential values. The bright red hues highlight areas of highest electronegativity, while the calm blue shades indicate regions of greater positive electrostatic potential. This detailed mapping reveals

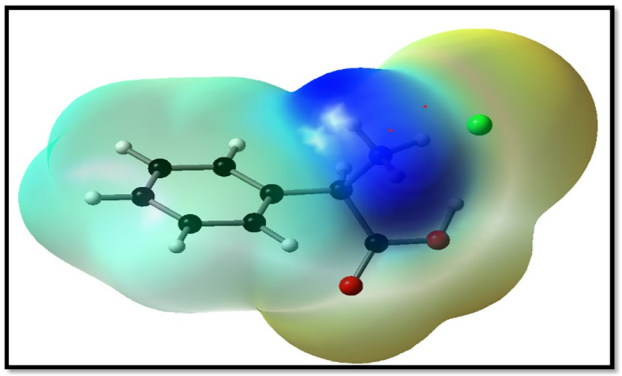

Fig. 5 Molecular electrostatic potential (MEP) surface of DPGCL

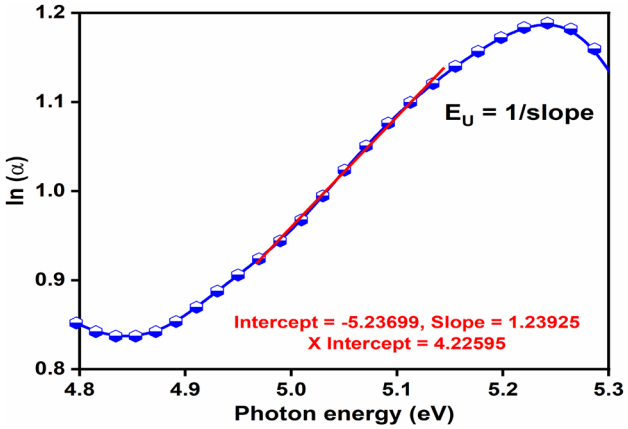

Fig. 6 ln (α) vs Photon energy (hν)

that the formation of a negative electrostatic potential is due to the attraction of protons to the surrounding electron density (ED) cloud. Conversely, the positive electrostatic potential arises from the repulsion of protons by atomic nuclei. The MEP map of D-phenylglycine hydrochloride not only clarifies potential intramolecular interactions but also identifies the most reactive sites, enabling predictions of where electrophilic and nucleophilic attacks are most likely to happen. This thorough understanding of molecular behaviour emphasises the complex relationship between electronic structures and reactive pathways in chemical processes.

2.2.4 *Absorption band tail*

Optical absorption studies are crucial in materials science, particularly for evaluating the suitability of various materials for device fabrication. The optical absorption spectrum provides key information, including parameters such as the absorption coefficient, cut-off wavelength, and band gap. Near the optical band edge, a notable exponential region called the Urbach tail [18] appears. A minimal tail reflects a highly ordered crystal structure. The relationship between the absorption coefficient (α) and photon energy (hυ) near the optical band edge is described by the Urbach empirical formula, expressed as: (2)

$$\alpha = \alpha_o \exp\left(\frac{h\nu}{E_u}\right) \tag{2}$$

here, α_o acts as a constant, while E_u is known as the Urbach energy. Taking the logarithm of both sides transforms the equation into a linear form: (3)

$$\ln(\alpha) = \ln\left(\alpha_o\right) + \frac{h\nu}{E_u} \tag{3}$$

The Urbach energy, or band tail energy, can be accurately determined by calculating the inverse of the slope from the plot of photon energy versus ln(α). As shown in Fig. 6, the Urbach energy is measured at 0.858 eV. A relatively low value indicates good crystalline quality, suggesting the material's potential for use in optoelectronic applications and advanced manufacturing processes. This energy level implies the material has favourable optical properties, making it suitable for high-performance devices such as lasers and photodetectors [19].

2.2.5 *Determination of optical constant*

Materials with a desirable refractive index are essential for fabricating various advanced devices, including organic light-emitting diodes (OLEDs), anti-reflective coatings for high-performance lenses, and sophisticated optical sensors. To thoroughly evaluate the optical response of these materials, it is essential to assess key optical constants, including the refractive index, extinction coefficient, optical conductivity, and electrical conductivity. The refractive index of a material depends on several factors, including the wavelength of incident light, the composition of the crystalline structure, carrier concentration, and temperature variations [20]. The extinction coefficient (K), a vital parameter that indicates how easily the material absorbs light, can be mathematically expressed as a function of the absorption coefficient (α) and the wavelength (λ) of the incident radiation, as shown in Eq. (4)

$$K = \frac{\alpha\lambda}{4\pi} \tag{4}$$

Figure 7a clearly shows that the extinction coefficient rises linearly as photon energy increases, emphasising the material's optical properties. The refractive index (n) can be given by Eq. (5)

$$n = \frac{-(R+1) \pm \sqrt{(-3R^2 + 10R - 3)}}{2(R-1)} \tag{5}$$

In examining the relationship between the refractive index (n) and reflectance (R), we observe that this connection can be graphically represented (Fig. 7b). From this data, the linear refractive index is found to be 1.371. This value is essential as it highlights the material's potential for applications in optical limiting and various optoelectronic devices [21].

Optical conductivity indicates how a material responds to different light intensities, showing its dynamic behaviour when exposed to radiation. The relationship governing optical conductivity can be expressed using Eq. (6),

$$\sigma_{op} = \frac{Knc}{\lambda} \tag{6}$$

where K represents the extinction coefficient, n is the refractive index, c is the speed of light in a vacuum, and λ is the wavelength of incident light. The findings shown in Fig. 8a reveal the correlation between optical conductivity and photon energy, marked by distinctive peaks that indicate enhanced electron transitions at specific energy levels. Such insights are crucial for optimising the material's efficiency in various photonic devices [22].

From these observations, we can infer that the optical conductivity of the material is closely related to its extinction coefficient and refractive index. Furthermore, a significant increase in the material's photoconductivity indicates a change in the absorption coefficient. The link between optical conductivity and photon energy also demonstrates that the material exhibits a strong photo responsive nature, suggesting that these optical parameters influence electrical conductivity. The electrical conductivity (σ_{ele}) directly relates to the optical conductivity (σ_{op}), as described in Eq. (7).

$$\sigma_{ele} = \frac{2\lambda\sigma_{op}}{\alpha} \tag{7}$$

Further analysis, as shown in Fig. 8b, reveals the inverse relationship between photon energy and electrical conductivity, indicating that as photon energy increases, the electrical conductivity of the material tends to decrease. These findings emphasise the importance of optimising photon energy to enhance the effectiveness of devices made from this material towards the photonic and electronic technologies [23].

2.3 Photoluminescence (PL) studies

The photoluminescence examination of the synthesised compound was conducted using an advanced Fluorolog-3-11 spectrometer. This sophisticated

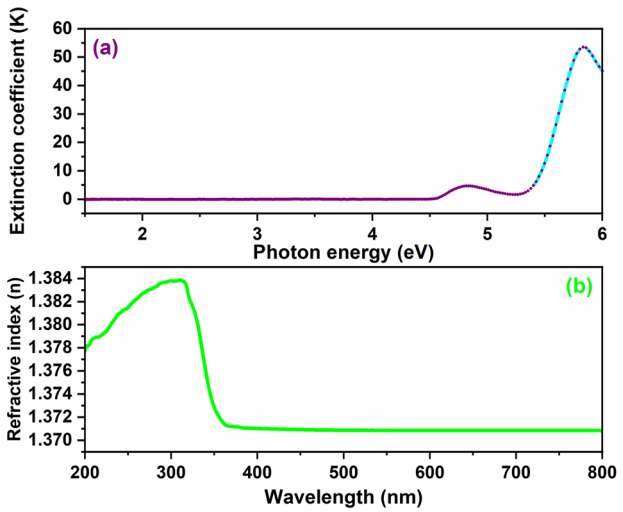

Fig. 7 **a** Extinction coefficient (K) vs Photon energy (hν), **b** Refractive index (n) vs Wavelength (nm)

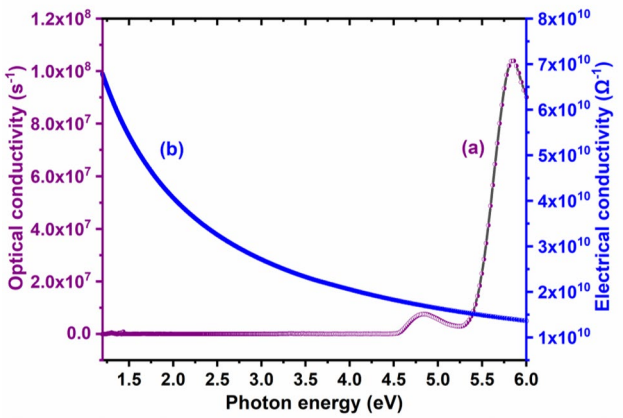

Fig. 8 **a** Optical conductivity (σ_{op}) vs Photon energy ($h\nu$), **b** Electrical conductivity (σ_{ele}) vs Photon energy ($h\nu$)

instrument produces illumination through a powerful 450-W xenon lamp, enabling a remarkable resolution of 0.2 nm across a broad wavelength range from 180 to 850 nm. Photoluminescence (PL) is characterised as the spontaneous emission of light following photoexcitation, a phenomenon that occurs when atoms transition between different energy levels due to absorbed photons [24]. The PL spectrum of the compound, which is in Fig. 9, was carefully recorded within the wavelength range of 220–450 nm. The material was intentionally excited at a precise wavelength of 228 nm. In the photoluminescence spectrum **(**Fig. 9**)**, a distinctly defined emission peak is observed within the ultraviolet region, specifically between 260 and 330 nm. The observation of a distinct and well-defined emission peak can be attributed to the radiative recombination of charge carriers within the material's band gap or to excitonic transitions between energy levels. This prominent emission peak is closely related to the π-π* electronic transition associated with the aromatic ring in the phenyl group, emphasising the molecular complexity involved. The sharpness of the peak indicates a highly ordered crystalline structure with minimal defects that could hinder nonradiative recombination processes. This implies that the material has excellent optical quality, enhancing its performance in specific applications. Additionally, the emission within this spectral range further confirms the wide band gap of the semi-organic material, boosting its potential for various advanced ultraviolet photonic and optoelectronic applications. [25].

2.4 HR-SEM/EDAX analysis

The surface morphology of the material was carefully examined with a Quanta 200FEG high-resolution scanning electron microscope (HR-SEM). As shown in Fig. 10, the HR-SEM images display detailed features of the material at various magnifications, specifically at × 2500, × 5000, × 10,000, and × 20,000, all taken at an acceleration voltage of 30 kilovolts. These images reveal a very smooth surface texture, with only a few microcrystalline structures, notably elongated cuboids that highlight the material's refined quality. This suggests a high degree of uniformity and excellence in the material's composition [26].

Additionally, the EDAX spectrum derived from the analysis, as illustrated in Fig. 11, reveals the elemental composition of the compound, identifying key elements such as carbon, nitrogen, oxygen, and chlorine. A detailed enumeration of the constituent elements, along with their corresponding weight percentages, highlights the successful synthesis of the mixture of D-phenylglycine and hydrochloric acid, confirming that the material is free from impurities. Furthermore, the consistent crystalline form of the synthesised compound reinforces its purity, indicating a stable and well-ordered molecular structure, which is essential for its potential applications.

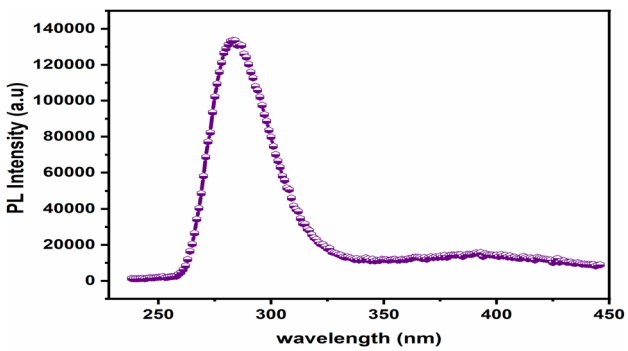

Fig. 9 PL Spectrum of DPGCL

2.5 Thermal analysis

Thermogravimetric differential thermal analysis (TG–DTA) is a sophisticated technique used to examine a material's thermal characteristics in detail, revealing critical parameters such as its melting point, the rate of heat change over time, and various transitions in heat energy. In this study, the TG–DTA analysis of the specified substance was performed within a temperature range of 25–400 °C at a controlled rate of 10 K/min using a NETZSCH STA 409C analyser under a nitrogen atmosphere to prevent oxidation and ensure accuracy. From the TGA/DTA curve (Fig. 12.), it is evident that the grown crystal decomposes in three distinct stages. A significant weight loss of approximately 51% occurs between 213 and 250 °C, with an endothermic peak at 213 °C. This loss is likely due to the release of trapped solvent molecules and volatile components. The decomposition of the organic part of the crystal results in a 38% weight loss in the range of 250–296 °C, accompanied by strong endothermic peaks at 246 and 286 °C. These peaks can be attributed to the thermal decomposition or phase transformation of the crystal. However, the substantial 38% weight loss suggests breakdown of the organic molecule, releasing CO_2 and NH_3 from the amino acid group. Beyond 296 °C, no

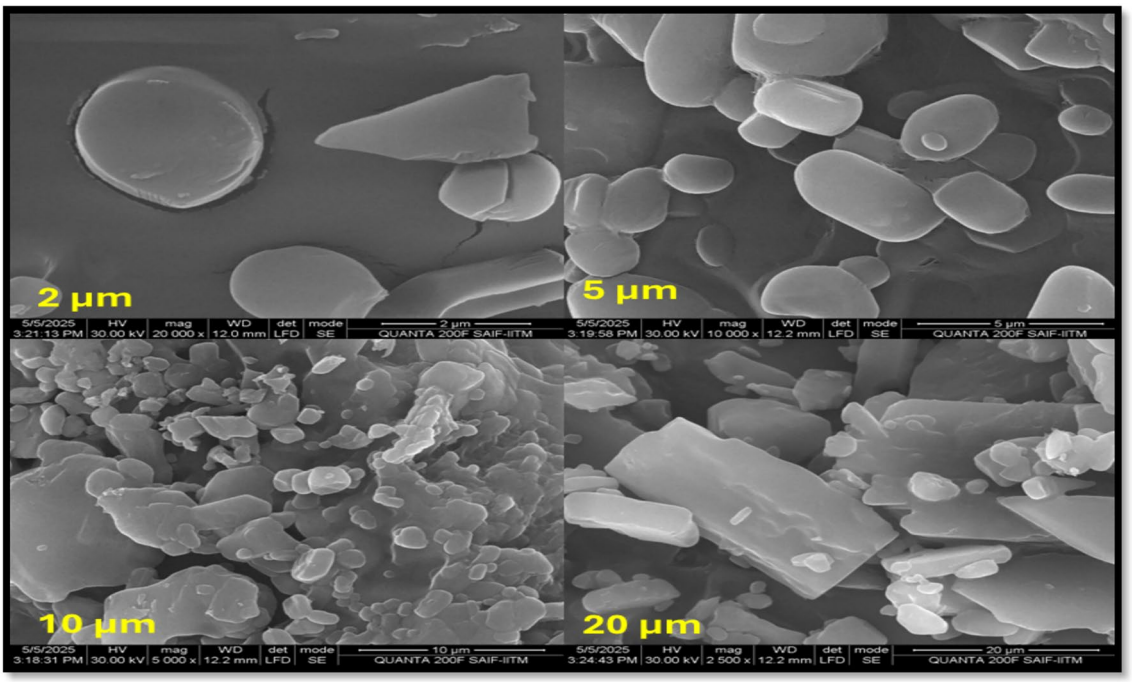

Fig. 10 HR-SEM images of DPGCL

Fig. 11 EDAX spectrum of DPGCL

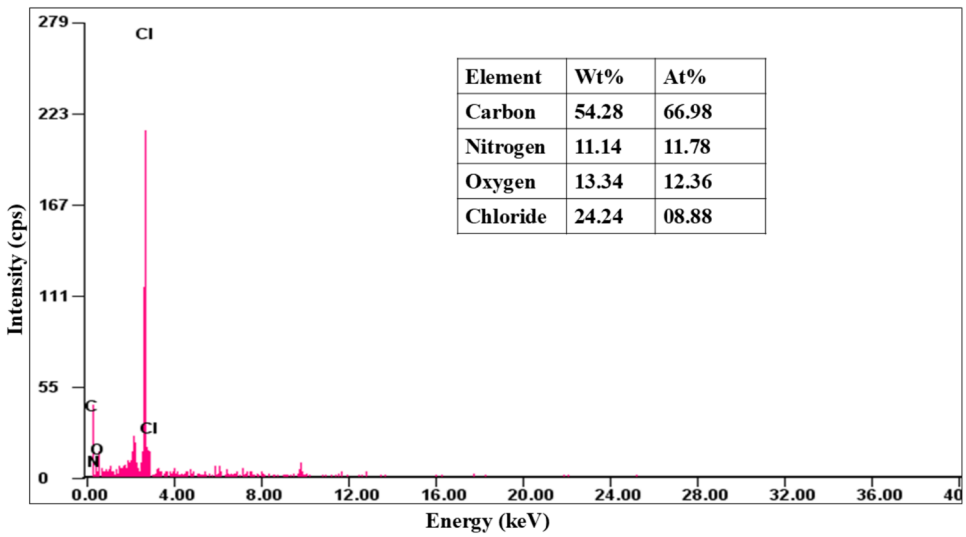

Element	Wt%	At%
Carbon	54.28	66.98
Nitrogen	11.14	11.78
Oxygen	13.34	12.36
Chloride	24.24	08.88

further weight loss is observed; the TGA curve indicates the formation of a thermally stable residue. The DTA curve shows only endothermic peaks, confirming dehydration, decomposition, and lattice breakdown during heating. The absence of exothermic peaks indicates that no oxidation reaction occurs in the grown crystal [27, 28]. These findings indicate not only the thermal transitions experienced by the material but also its remarkable thermal stability. This exceptional stability demonstrates the compound's ability to withstand high laser power applications.

2.6 Laser damage threshold studies

The inherent tolerance of crystals to laser irradiance is influenced by a myriad of factors, including the purity of the material, its structural characteristics, the phenomenon of multiple-photon ionisation, and

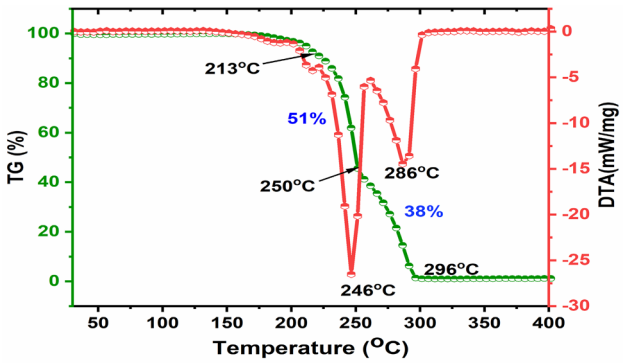

Fig. 12 TG–DTA plot of DPGCL

the critical damage threshold associated with these processes. Materials that demonstrate heightened resilience to laser exposure hold considerable promise for transformative applications in the field of material science [29]. To evaluate the laser damage threshold of DPGCL, a precise experimentation setup was employed, utilising a Q-switched Nd-YAG laser of 1064 nm. This powerful laser delivers pulses with a width of 10 ns and operates at a frequency of 10 Hz, making it particularly effective for such assessments. A focussed laser beam, measuring 1 mm in diameter, was meticulously directed onto the impeccably polished surface of the crystal through a converging lens with a focal length of 10 cm. The energy output from the laser source was precisely adjusted using a variable attenuator, enabling an accurate assessment of the material's resilience at varying energy levels. During exposure to these differing energy intensities, observable damage to the crystal surface was noted, as depicted in Fig. 13. This damage is primarily attributed to the thermal stress that builds up within the material's lattice, indicating a critical failure point. To better understand this phenomenon, the power density was determined using the specified Eq. (8).

$$P_d = \frac{E_p}{\tau \pi {\omega_0}^2} \tag{8}$$

The resulting power density values were then compared with those of other nonlinear optical (NLO) materials, as demonstrated in Table 2. Further investigation emphasises that the thermal stability of the material is a crucial factor in its performance. The crystal's ability to maintain its structural integrity under extreme conditions positions it as a leader in ongoing developments within photonic technology and related fields [30].

2.7 Second order nonlinear optical studies

The second-harmonic generation (SHG) conversion efficiency of the sample was carefully evaluated using the Kurtz-Perry powder technique, a widely recognised method in the field [35]. For this analysis, powdered potassium dihydrogen phosphate (KDP) served as a standard reference material, given its well-established SHG properties. A high-intensity, Q-switched Nd: YAG laser emitting a fundamental wavelength of 1064 nm was used as the optical source for the experiment. This powerful laser is known for its effectiveness

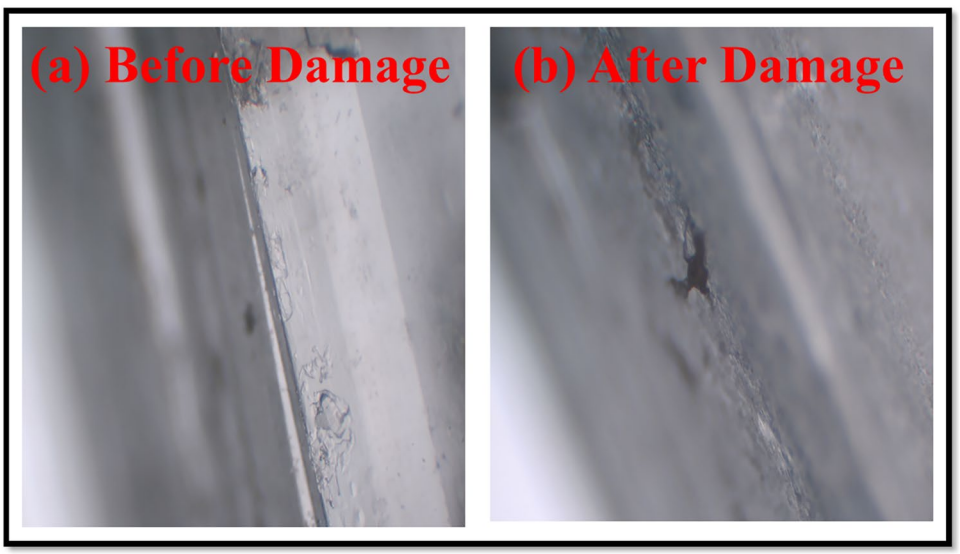

Fig. 13 Laser damage view pattern **a** before, **b** after

Table 2 Comparison of the LDT value with other NLO materials

NLO materials	Power density (GW/cm^2)
KDP [31]	0.20
Bis-glycine hydrochloride [32]	1.62
γ-glycine [33]	1.92
Diglycine picrate [34]	3.36
D-phenylglycine hydrochloride [present work]	5.46

Table 3 SHG efficiency of various semi-organic materials concerning KDP

Nonlinear optical materials	SHG efficiency	Crystal system
(Tri) glycine barium chloride [37]	0.5	Orthorhombic
L-Glycine thiourea [38]	0.6	Orthorhombic
Diglycine hydrobromide [39]	0.8	Orthorhombic
D-phenylglycine hydrochloride [present study]	1.3	Orthorhombic

in producing nonlinear optical effects. As expected, the SHG process was confirmed by the detection of green light at 532 nm, clearly indicating the material's nonlinear optical response. At an input energy of 0.7 J, the SHG output for the compound was an impressive 7.2 mJ, significantly exceeding the KDP reference, which recorded an output of 5.4 mJ. This notable result showed that the SHG efficiency of the tested material was 1.3 times greater than that of KDP, demonstrating its superior nonlinear optical performance and is compared with other NLO materials as shown in Table 3. Additionally, it was observed that the SHG efficiency tends to increase with larger particle size [36], suggesting that optimising particle dimensions could lead to further improvements in SHG efficiency.

2.8 Third-order NLO studies (Z-scan) analysis

The non-centrosymmetric material under investigation showcases the remarkable ability to propagate both second-order and third-order nonlinear optical properties [40]. To assess the efficiency of the third-order nonlinear optical (NLO) responses, the Z-scan technique, an established method pioneered by Bahae [41], was employed. This technique has gained widespread recognition as the standard approach for evaluating the third-order NLO characteristics of various materials. A meticulous investigation into the nonlinear absorption coefficient and the optical limiting threshold of the material was conducted using open-aperture Z-scan methods, enabling a comprehensive analysis of the optical limiting parameters. This experimental setup utilised a Q-switched Nd: YAG laser system (Quanta-Ray INDI-10), characterised by a pulse width of 9 ns and a wavelength of 532 nm. To prepare the sample for testing, 0.15 mg of the powdered material was skillfully dispersed in 5 ml of ethyl glycol, achieving a linear transmittance of 70%. Ethylene glycol primarily serves as a polar solvent, enhancing the activity of solutes while exhibiting no notable nonlinear optical response. A Z-scan conducted under the specified experimental conditions on pure ethylene glycol reveals an absence of nonlinear characteristics. Consequently, it does not affect the nonlinear absorption of the DPGCL sample. The essential parameters beam waist (ω_0), Rayleigh range (Leff), and pulse width were precisely defined as 16.9 μm, 1.69 mm, and 100 μJ, respectively. A focused beam intensity of 2.46×10^{12} W/m^2 was meticulously directed into the sample holder through a converging lens with a focal length of 15 cm. The experimental procedure involved systematically scanning the beam across a distance of 100 mm in carefully predetermined increments. This approach highlighted the intricate relationship between the absorption coefficient and the corresponding increase in light intensity [42]. The observed characteristics of peaks and valleys demonstrated clear evidence of nonlinear optical behaviour at elevated input fluence levels, while the shoulder features indicated linear transmittance at lower intensities. Figure 14 vividly illustrates the open aperture curve of DPGCL, with normalised transmission values derived using Eq. (9),

$$T(z) = \frac{1}{\sqrt{\pi q(z)}} \int_{-\infty}^{+\infty} \ln\left[1 + q(z)\exp\left(-\tau^2\right)\right] d\tau \tag{9}$$

where $q(z) = \beta L_{\text{eff}} \frac{I_o}{\left(1+(Z/Z_o)^2\right)}$, β is the nonlinear absorption coefficient, Z_o is the Rayleigh range or diffraction length, Io is the input intensity of the laser beam, and L_{eff} is the effective length of the sample. The nonlinear absorption in DPGCL is attributed to the two-photon absorption process, with theoretical and experimental data findings aligning with each other. The fluence

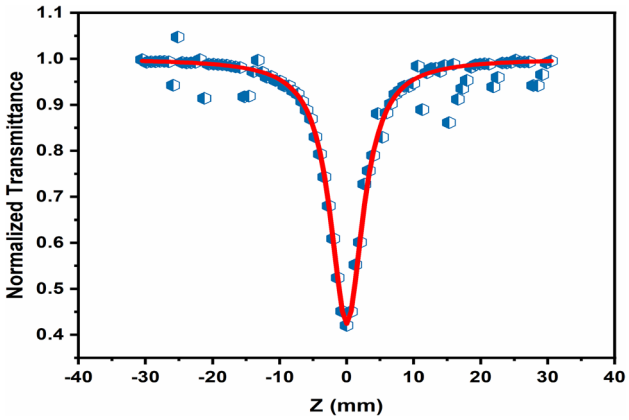

Fig. 14 Open aperture curve of DPGCL

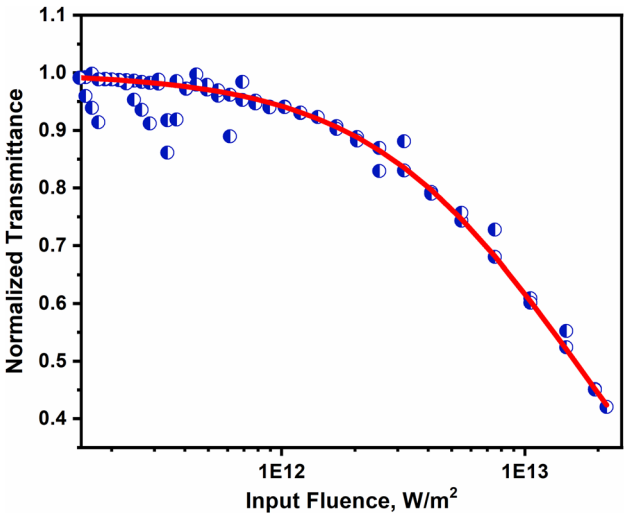

Fig. 15 Normalised transmittance vs input intensity (W/m.^{2})

(F(z)) of a filtered Gaussian laser beam at position Z is described by an Eq. (10) derived from the open-aperture Z-scan data.

$$F(z) = 4\sqrt{\ln 2}\left(\frac{E_{in}}{\pi\frac{3}{2}}\right)\omega(z)^2 \tag{10}$$

The beam radius can be characterised using Eq. (11), which further elucidates the system's behaviour.

$$\omega(Z) = \omega(0)\left[1 + \left(\frac{z}{z^o}\right)^2\right]^{1/2} \tag{11}$$

Notably, the open-aperture curve, corresponding to an on-axis input intensity of 2.46×10^2 W/m^2, indicates that the DPGCL crystal exhibits intriguing optical limiting behaviour attributed to reverse saturable absorption. Figure 15 effectively illustrates the relationship between normalised transmittance and input intensity (W/m^2), highlighting the optical limiting characteristics of the material, which has an onset threshold of 2.89×10^{12} W/m^2. Lowering this threshold improves the effectiveness of the optical limiting effect. Table 4 provides a comprehensive collection of data, including the nonlinear optical absorption coefficient (β), saturation intensity (I_s), and the onset limiting threshold for the material. The third-order nonlinear absorption coefficient of the material is compared with that of other NLO materials, as presented in Table 5. This comparison indicates that the material demonstrates a promising third-order NLO efficiency. The results from the Z-scan technique show a significant increase in third-order nonlinearity, opening up potential applications in the dynamic fields of photonics and optoelectronics [43, 44].

Table 4 Third-order NLO parameters of DPGCL

Sample Name	Saturation Intensity $I_s \times 10^{11}$ W/m^2	Nonlinear absorption coefficient $\beta \times 10^{-10}$ m/W	Onset optical limiting threshold $\times 10^{12}$ W/m^2
DPGCL	32	0.87	2.89

Table 5 Comparison of nonlinear absorption coefficient with other NLO materials

Nonlinear optical materials	Nonlinear absorption coefficient $\beta \times 10^{-10}$ m/w
Thiosemicarbazide [45]	0.31
Creatininium phthalate [46]	0.54
Methyl triphenylphosphonium bromide [47]	0.59
D-phenylglycine hydrochloride [present study]	0.87

3 Conclusion

A high-quality single crystal of D-phenylglycine hydrochloride was successfully synthesised using the slow evaporation technique, followed by an extensive analysis of its structural, optical, thermal, and

nonlinear optical properties. Single-crystal X-ray diffraction (XRD) confirmed that the material belongs to the orthorhombic crystal system. Ultraviolet–Visible (UV–Vis) spectroscopy demonstrated a distinct cut-off wavelength at 228 nm, accompanied by an optical band-gap of 5.4 eV. The material's stability and suitability for optoelectronic applications were underscored by the examination of its electrical structure, supported by HOMO–LUMO and Molecular Electrostatic Potential (MEP) analyses. Photoluminescence spectroscopy indicated the material's potential effectiveness for device fabrication. High-Resolution Scanning Electron Microscopy (HR-SEM) and Energy Dispersive X-ray Analysis (EDAX) validated the smooth surface morphology and the precise elemental composition. Furthermore, Thermogravimetric Analysis (TGA) and Differential Thermal Analysis (DTA) confirmed the excellent thermal stability of the material, with a melting point recorded at 286 °C. Noteworthy is the material's second-order nonlinear optical efficiency, which is 1.3 times greater than that of potassium dihydrogen phosphate (KDP), in addition to a high laser damage threshold of 5.46 GW/cm^2. The material's applicability for nonlinear optical and laser-based technologies is further enhanced by its third-order nonlinear properties, which include a nonlinear absorption coefficient of 0.87×10^{-10} m/W, saturation intensity of 32×10^{11} W/m^2, and a limiting threshold of 2.89×10^{12} W/m^2. D-phenylglycine hydrochloride presents itself as a promising candidate for advanced photonic and optoelectronic applications, owing to its remarkable nonlinear performance, optical transparency, thermal stability, and structural integrity.

Acknowledgements

The authors sincerely thank Vels Institute of Science, Technology and Advanced Studies (VISTAS), Pallavaram, Chennai-600117, for supporting this research. We also appreciate the valuable contributions of SAIF and IIT-Madras for their assistance in conducting single-crystal X-ray diffraction, UV-visible, Photoluminescence, HR-SEM/EDAX, and TG-DTA analyses.

Author contributions

P. Hemalatha: Conceptualisation, Methodology, Data curation, and Writing–original draft. M Mohanraj: Methodology, Writing–review and editing, Validation, Data curation. M Lakshmipriya: Writing–review and editing, Validation, Formal analysis, Data curation. T.C. Sabari Girisun: Writing–review and editing, Validation, Formal analysis, Data curation. P. Jayaprakash: Writing–review and editing, Validation, Formal analysis, Data curation. M Parthasarathy: Methodology, Data curation, Investigation, Supervision, and Validation.

Funding

The authors did not receive support from any organisation for the submitted work.

Data availability

The data presented in this study are available upon request from the corresponding author.

Declarations

Conflict of interests The authors declare no competing interests.

Ethical approval All experiments were carried out according to university guidelines. None of the authors used human beings as research subjects.

Consent for publication In the present study, there were no person's data in any form.

References

1. C.R. Kagan, D.B. Mitzi, C.D. Dimitrakopoulos, Organic-inorganic hybrid materials as semiconducting channels in thin-film field-effect transistors. Science **286**, 945 (1999). https://doi.org/10.1126/science.286.5441.945
2. J. Zyss, Ed., Molecular Nonlinear Optics: Materials, Physics and Devices. Academic Press, Boston (1994). https://doi.org/10.1002/adma.19950070232
3. K. Bouchouit, Z. Sofiani, N. Benali-Cherif, L. Bendheif, A. Migalska-Zalas, I.V. Kityk, Third-order nonlinear optical properties of hybrid mono crystals with n-conjugated systems. 2005 7th International Conference Transparent

Optical Networks, Barcelona **2**, 367–371 (2005). https://doi.org/10.1109/ICTON.2005.1506175
4. J. Cheng, Xu. Guochao, R. Han, J. Dong, Ye. Ni, Efficient access to L-phenylglycine using a newly identified amino acid dehydrogenase from *Bacillus clausii*. RSC Adv. **6**, 80557 (2016). https://doi.org/10.1039/C6RA17683F
5. Ł Wołoszyn, M.M. Ilczyszyna, V. Kinzhybalo, The dehydration process in the DL-phenylglycinium trifluoromethanesulfonate monohydrate crystal revealed by XRD, vibrational and DSC studies. Acta Cryst. C **75**, 1569–1579 (2019). https://doi.org/10.1107/S2053229619014402
6. M. Parthasarathy, K. Arun Kumar, R. Gopalakrishnan, D-phenylglycinium bromide. Acta Crystallogr. Sect. E Struct. Rep. Online **69**, 470 (2013). https://doi.org/10.1107/S1600536813004807
7. K. Bouchouit, L. Bendheif, N. Benali-Cherif, D-phenylglycinium nitrate. Acta Cryst. E **60**, 272–274 (2004). https://doi.org/10.1107/S1600536804000972
8. S. Ramasamy, B. Sridhar, V. Ramakrishnan, R.K. Rajaram, D-phenylglycinium perchloride. Acta Cryst. E **57**, 1149–1151 (2001). https://doi.org/10.1107/S160053680101858X
9. N. Srinivasan, B. Sridhar, R.K. Rajaram, Bis(D-phenylglycinium) sulfate monohydrate. Acta Cryst. E **57**, 754–756 (2001). https://doi.org/10.1107/S1600536801011941
10. S. Ravichandran, J.K. Dattagupta, C. Chakrabarti, D-phenylglycine hydrochloride. Acta Cryst. C **54**, 499–501 (1998). https://doi.org/10.1107/S0108270197014674
11. M. Picollo, M. Aceto, T. Vitorino, UV–Vis spectroscopy. Phys. Sci. Rev. **4**, 2018–0008 (2019). https://doi.org/10.1515/psr-2018-0008
12. S. Moshtaghi, S. Zinatloo-Ajabshir, M. Salavati-Niasari, Nanocrystalline barium stannate: facile morphology-controlled preparation, characterization and investigation of optical and photocatalytic properties. J. Mater. Sci. Mater. Electron. **27**, 834–842 (2016). https://doi.org/10.1007/s10854-015-3824-3
13. S.R. Meeraa, M. Parthasarathy, Synthesis and characterisation of single crystals of creatininium hydrochloride for third-order NLO applications. Cryst. Res. Technol. **59**, 2300133 (2024). https://doi.org/10.1002/crat.202300133
14. M. Mohanraj, M. Parthasarathy, A comprehensive evaluation of nonlinear optical materials: synthesis, growth, spectral, photoluminescence, LDT, photoconductivity, thermal, antibacterial and second harmonic generation analysis. Solid State Commun. **404**, 116113 (2025). https://doi.org/10.1016/j.ssc.2025.116113
15. P. Jayaprakash, P. Sangeetha, M. Peer Mohamed, G. Vinitha, S. Muthu, M. Prakash, M. Lydia Caroline, Growth and characterization of DL-mandelic acid ($C_6H_5CH(OH)CO_2H$) single crystal for third-order nonlinear optical applications. J. Mol. Struct. **1148**, 314–321 (2017). https://doi.org/10.1016/j.molstruc.2017.07.049
16. I. Dhifallah, S.B. Slama, A. Bardaoui, R. Chtourou, A combined experimental and density functional theory study of calcination temperature effects on the properties and photocatalytic activity of starch-mediated spinel $ZnAl_2O_4$. J. Inorg. Organom. Polym. Mater. (2025). https://doi.org/10.1007/s10904-025-04003-z
17. P. Jayaprakash, M. Lydia Caroline, S. Sudha, R. Ravisankar, G. Vinitha, P. Ramesh, E. Raju, Synthesis, growth, optical and third order nonlinear optical properties of l-phenylalanine d-mandelic acid single crystal for photonic device applications. J. Mater. Sci. Mater. Electron. **31**, 20460–20471 (2020). https://doi.org/10.1007/s10854-020-04565-3
18. S. Benramache, Y. Aoun, S. Lakel, B. Benhaoua, C. Torchi, The calculate of optical gap energy and urbach energy of Ni12xCoxO thin films. Indian Acad. Sci. (2019). https://doi.org/10.1007/s12046-018-1003-y
19. G.G. Riungu, S.W. Mugo, J.M. Ngaruiya, G.M. John, N. Mugambi, Optical band energy, Urbach energy and associated band tails of nano crystalline TiO_2 films at different annealing rates. Am. J. Nanosci. **7**, 28–34 (2021). https://doi.org/10.11648/j.ajn.20210701.15
20. R. Bhatt, I. Bhaumik, S. Ganesamoorthy, A.K. Karnal, M.K. Swami, H.S. Patel, P.K. Gupta, Urbach tail and bandgap analysis in near stoichiometric LiNbO3 crystals. Phys. Status Solidi A **1**, 176–180 (2012). https://doi.org/10.1002/pssa.201127361
21. O. Belahssen, H.B. Temam, S. Lakel, B. Benhaoua, S. Benramache, S. Gareh, Effect of optical gap energy on the Urbach energy in the undoped ZnO thin films. Optik **126**, 1487–1490 (2015). https://doi.org/10.1016/j.ijleo.2015.04.010
22. K. Subramani, P.S. Joseph, G. Shankar, Optical, electrical and ac conductivity measurements of nonlinear optical dimethylaminomethylphthalimide doped with cadmium chloride single crystal for nano applications. Opt. Commun. **300**, 12–16 (2013). https://doi.org/10.1016/j.optcom.2013.03.009
23. K. Rajesh, P. Krishnan, A. Mani, K. Anandan, K. Gayathri, P. Devendran, Physical strength and opto-electrical conductivity of L-serine phosphate single crystal for structural and photonics devices fabrication. Mater. Res. Innov. (2019). https://doi.org/10.1080/14328917.2019.1664178
24. M. Daoudi, H. Kaouach, I. Dhifallah, A. Ouerghi, R. Chtourou, Optical band-gap shift in (InAs)GaAs/AlGaAs HEMTs structures studied by photoluminescence spectroscopy. Optik **126**, 932–936 (2015). https://doi.org/10.1016/j.ijleo.2015.02.087

25. F. Yogam, I. Vetha Potheher, R. Jeyasekaran, M. Vimalan, M. Antony Arockiaraj, P. Sagayaraj, Growth, thermal, and optical properties of L-asparagine monohydrate NLO single crystal. J. Therm. Anal. Calorim. **114**, 1153–1159 (2013). https://doi.org/10.1007/s10973-013-3138-8
26. D. Majumdar, J.E. Philip, A. Dubey, A. Tufail, S. Roy, Synthesis, spectroscopic findings, SEM/EDX, DFT, and single-crystal structure of Hg/Pb/Cu–SCN complexes: in silico ADME/T profiling and promising antibacterial activities. Heliyon **8**, 16103 (2023). https://doi.org/10.1016/j.heliyon.2023.e16103
27. B. Uma, K. Sakthi Murugesan, S. Krishnan, R. Jayavel, B. Milton Boaz, Growth, optical, thermal and dielectric studies of a highly polarisable semi organic NLO crystal: bis D-phenyl glycinium sulphate monohydrate. Mater. Chem. Phys. **142**, 659–666 (2013). https://doi.org/10.1016/j.matchemphys.2013.08.018
28. A. Bardaoui, I. Dhifallah, M. Daoudi, S. Aouini, M. Amlouk, R. Chtourou, Exploring the impact of annealing temperature on morphological, structural, vibrational and electron paramagnetic resonance properties of starch-mediated spinel $CoAl_2O_4$: experimental and DFT study. J. Solid State Chem. **335**, 124732 (2024). https://doi.org/10.1016/j.jssc.2024.124732
29. M. Shakir, S.K. Kushwaha, K.K. Maurya, R.C. Bhatt, Rashmi, M.A. Wahab, G. Bhagavannarayana, Unidirectional growth of l-proline cadmium chloride monohydrate single crystal and its characterization for structural, vibrational, LDT, optical and dielectric properties. Mater. Chem. Phys. **120**, 566–570 (2010). https://doi.org/10.1016/j.matchemphys.2009.12.008
30. S. Vediyappan, A. Raja, R.M. Jauhar, R. Kasthuri, V. Vijayan, M. Senthil Pandian, R. Perumalsamy, V. Gandhiraj, Synthesis, crystal growth, structure, crystalline perfection, thermal, linear, and nonlinear optical investigations on 2-amino-5-nitropyridine 4-chlorobenzoic acid (1:1): a novel organic single crystal for NLO and optical limiting applications. J. Mater. Sci. Mater. Electron. **32**, 15026–15045 (2021). https://doi.org/10.1007/s10854-021-06056-5
31. Y. Hu, Z. Zhu, J. Xiao, H. Shao, L. Zhao, M. Xu, J. Zhuang, Atomic scale study of stress-induced misaligned subsurface layers in KDP crystals. Sci. Rep. **9**, 10399 (2019). https://doi.org/10.1038/s41598-019-46672-0
32. L. Gobinathan, K. Boopathy, Photoluminescence, laser damage threshold, optical transmittance, FTIR, mechanical, dielectric, thermal and XRD studies on bis – glycine hydrochloride single crystal. J. Adv. Chem. **12**, 4523–4535 (2016)
33. S. Gracelin Juliana, P. Sathishkumar, S.C. Vella Durai, Crystal growth and characterization of an efficient nonlinear optical material: γ-glycine crystal. Indian J. Pure Appl. Phys. **62**, 1098–1105 (2024). https://doi.org/10.56042/ijpap.v62i12.9843
34. R. Suganthi, K. Balasubramanian, Multifaceted characterization of diglycine picrate (DGP) single crystals: exploring growth, mechanical, optical, thermal, electrical, and laser damage threshold properties for advanced nonlinear optical applications. Int. Res. J. Multidisc. Scope **6**, 1014–1029 (2025). https://doi.org/10.47857/irjms.2025.v06i03.04551
35. M. Sun, G. Wang, J. Yao, The Kurtz-Perry powder technique revisited: a study of the effect of reference selection on powder second-harmonic generation response. Molecules **28**, 1116 (2023). https://doi.org/10.3390/molecules28031116
36. M. Parthasarathy, R. Gopalakrishnan, Growth, photoluminescence, thermal and mechanical behaviour of ethyltriphenylphosphonium bromide dihydrate crystal. Opt. Mater. **35**, 2056–2061 (2013). https://doi.org/10.1016/j.optmat.2013.05.007
37. S. Chennakrishnan, S.M. Ravi Kumar, D. Sivavishnu, M. Ganapathi, I. Vetha Potheher, M. Vimalan, Synthesis, growth and characterization of (tri) glycine barium chloride single crystal for applications in the domain of optoelectronics and photonics. J. Mater. Sci. Mater. Electron. **27**, 10113–10121 (2016). https://doi.org/10.1007/s10854-016-5086-0
38. S. Arockia Avila, A. Leo Rajesh, Growth and characterization of L-Glycine thiourea nonlinear optical single crystal for optoelectronic applications. J. Mater. Sci. Mater. Electron. **28**, 10893–10901 (2017). https://doi.org/10.1007/s10854-017-6868-8
39. B. Narayana Moolya, S.M. Dharmapraksh, Growth and characterization of nonlinear optical diglycinehydrobromide single crystals. Mater. Lett. **61**, 3559–3562 (2007). https://doi.org/10.1016/j.matlet.2006.11.117
40. H. Algarni, A.A. Alshahrani, A.E. Al-Salami, Improving structural, UV–visible, SHG efficiency, third order nonlinear optical, mechanical, thermal and dielectric properties of ZTC crystal using π bonded ligand of oxalic acid. Opt. Mater. **88**, 385–391 (2019). https://doi.org/10.1016/j.optmat.2018.11.046
41. M. Sheik-Bahae, A.A. Said, T.-H. Wei, D.J. Hagan, E.W. Van Stryland, Sensitive measurement of optical nonlinearities using a single beam. IEEE J. Quantum Electron. **26**, 760–769 (1990). https://doi.org/10.1109/3.53394
42. N. Mahalakshmi, S.R. Meeraa, G. Vinitha, M. Parthasarathy, Synthesis, growth, photoluminescence, thermal, and third-order nonlinear optical properties of glycine methyl ester hydrochloride single crystal for opto-electronic

applications. Braz. J. Phys. **54**, 49 (2024). https://doi.org/10.1007/s13538-024-01420-2

43. R. Ragu, M. Akilan, J.P. Angelena, P.S. Latha Mageshwari, S. Jerome Das, Growth, optical, mechanical, thermophysical, laser damage threshold (LDT) and Z-scan studies on dilithium succinate single crystal for optical limiting applications. J. Mater. Sci. Mater. Electron. **30**, 6287–6299 (2019). https://doi.org/10.1007/s10854-019-00933-w
44. T.A. Hegde, A. Dutta, G. Vinitha, $\chi^{(3)}$ measurement and optical limiting behaviour of novel semi-organic cadmium mercury thiocyanate crystal by Z-scan technique. Appl. Phys. A **124**, 808 (2018). https://doi.org/10.1007/s00339-018-2235-8
45. B. Thilaga Rajeswari, P. Sathya, P. Dhanasekaran, G. Vinitha, S. Meyvel, V. Vijayalakshmi, J. Aarthi, First-time investigation on crystal growth, optical, thermal, electrical and third-order non-linear optical activities of novel thiosemicarbazide single crystals for non-linear optical applications. J. Mater. Sci. Mater. Electron. **32**, 22984–22998 (2021). https://doi.org/10.1007/s10854-021-06783-9
46. S. Surya, B. Gunasekaran, T.C.S. Girisun, Synthesis, growth, crystal structure, thermal, optical, electrical and third-order nonlinear optical properties of creatininium phthalate as a new nonlinear optical single crystal. J. Mater. Sci. Mater. Electron. **33**, 8683–8701 (2022). https://doi.org/10.1007/s10854-021-06771-z
47. S. Hemavathy, G. SanthanaKrishnan, T.C. Sabari Girisun, M. Parthasarathy, Investigation on growth, structural, spectral, DFT, MEP computational studies of novel methyl triphenylphosphonium bromide hydrate single crystal for third-order nonlinear optical limiting applications. J. Mol. Struct. **1325**, 140968 (2025). https://doi.org/10.1016/j.molstruc.2024.140968